Effect of oxide supports on Pd–Ni bimetallic catalysts for 1,3-butadiene hydrogenation

ARTICLE *in* APPLIED CATALYSIS A GENERAL · NOVEMBER 2014

Impact Factor: 3.94 · DOI: 10.1016/j.apcata.2014.11.001

4 AUTHORS, INCLUDING:

Marc David Porosoff

United States Naval Research Laboratory

17 PUBLICATIONS **308** CITATIONS

SEE PROFILE

Tiefeng Wang

Tsinghua University

84 PUBLICATIONS **856** CITATIONS

SEE PROFILE

Applied Catalysis A: General 490 (2015) 17–23

Contents lists available at ScienceDirect

Applied Catalysis A: General

journal homepage: www.elsevier.com/locate/apcata

Effect of oxide supports on Pd–Ni bimetallic catalysts for 1,3-butadiene hydrogenation

Ruijun Hou[a,b], Marc D. Porosoff[b,c], Jingguang G. Chen[b,*], Tiefeng Wang[a,*]

[a] Beijing Key Laboratory of Green Reaction Engineering and Technology, Department of Chemical Engineering, Tsinghua University, Beijing 100084, China
[b] Department of Chemical Engineering, Columbia University, New York, NY 10027, USA
[c] Department of Chemical and Biomolecular Engineering, University of Delaware, Newark, DE 19716, United States

ARTICLE INFO

Article history:
Received 26 August 2014
Received in revised form 30 October 2014
Accepted 1 November 2014
Available online 8 November 2014

Keywords:
Support effect
Pd–Ni bimetallic catalysts
Selective hydrogenation
1,3-Butadiene

ABSTRACT

Our previous work showed that the Pd–Ni bimetallic catalyst had better hydrogenation activity and 1-butene selectivity in the selective hydrogenation of 1,3-butadiene. In the present work, the effect of oxide supports on the hydrogenation of 1,3-butadiene was studied over Pd–Ni bimetallic catalysts supported on γ-Al_2O_3, SiO_2, CeO_2, ZrO_2 and TiO_2. Transmission electron microscopy (TEM) and extended X-ray absorption fine structure (EXAFS) were used to characterize the particle size and the extent of Pd–Ni bimetallic bond formation, respectively. The support effect affected the bimetallic particle structure, but appeared to have no apparent influence in the hydrogenation activity. All the bimetallic catalysts showed ~100% selectivity to butenes; however, the supports affected the 1-butene selectivity. PdNi/γ-Al_2O_3 showed the highest 1-butene selectivity of ~80% at 1,3-butadiene conversions lower than 50% but decreased rapidly at higher conversion. The different performance of the supports in 1-butene selectivity might be attributed to strong metal-support interaction (SMSI), the oxygen defects and the geometric/electronic effect on the catalysts.

1. Introduction

Selective hydrogenation is one of the critical reactions to remove alkynes and dienes in the feedstock for polymer synthesis. The hydrocarbon streams from cracking units typically contain ~1% alkynes or dienes, which must be reduced to below 10 ppm for polymerization processes because they poison the catalysts and degrade the product quality [1,2]. For example, hydrogenation of 1,3-butadiene is used for the purification of butene streams. Among the products of 1,3-butadiene hydrogenation, 1-butene is the desired product for manufacturing polybutene. In this paper, 1,3-butadiene was chosen as a probe molecule to identify catalysts for the selective hydrogenation of one of the C=C bonds in dienes.

In our previous work on single crystal surfaces, the Pd-terminated, PdNiPd(1 1 1) surface was demonstrated to be more active and more selective to 1-butene than the Pd(1 1 1) surface for the hydrogenation of 1,3-butadiene using ultra-high vacuum (UHV) temperature programmed desorption (UHV-TPD) and density functional theory (DFT) calculations. The better performance of the Pd–Ni bimetallic surface was verified on γ-Al_2O_3 supported catalysts [3]. However, the extent of Pd–Ni bimetallic bond formation in PdNi/γ-Al_2O_3 was relatively small. The Pd–Ni coordination number was only 1.4 because most Ni atoms existed either in the form of $NiAl_2O_4$ or as Ni monometallic nanoparticles. It is very likely that the Pd–Ni bimetallic effect would be more pronounced by increasing the extent of Pd–Ni bimetallic bond formation. One possible way to increase the Pd–Ni coordination number is using oxide supports other than γ-Al_2O_3 on which the active metal would not form the spinel species.

Another motivation to study the support effect for the Pd–Ni bimetallic catalyst is the importance to identify a proper support for industrial application, with respect to the catalytic activity and selectivity. The interaction between the oxide supports and metal particles was previously shown to have a significant effect on the catalyst activity for hydrogenation reactions. For the hydrogenation of acetone over the Pt–Ni bimetallic catalysts, Qi et al. [4] reported that PtNi/SiO_2 had much higher activity than PtNi/γ-Al_2O_3 and PtNi/TiO_2. For the hydrogenation of 1,3-butadiene, Lonergan et al. [5] reported that the activity of Pt–Ni catalysts were similar on γ-Al_2O_3, α-Al_2O_3 and low surface area (LSA)-ZrO_2, while Pt–Ni supported on high surface area (HSA)-ZrO_2 showed much lower activity due to the strong metal-support interaction (SMSI). It was also reported that Pt–Ni/TiO_2 showed much lower activity

* Corresponding authors.
E-mail addresses: jgchen@columbia.edu (J.G. Chen), wangtf@tsinghua.edu.cn (T. Wang).

http://dx.doi.org/10.1016/j.apcata.2014.11.001
0926-860X/

than Pt–Ni/γ-Al_2O_3 due to the SMSI between the Pt particles and TiO_2 [6].

According to the literature above, the SMSI effect inhibits the hydrogenation activity of the Pt-based catalysts. In this work, the Pd–Ni bimetallic catalysts on several commonly used oxide supports were synthesized for the hydrogenation of 1,3-butadiene to study the support effect on the hydrogenation activity and selectivity. Transmission electron microscopy (TEM), CO chemisorption and extended X-ray absorption fine structure (EXAFS) were used to characterize the catalysts. The bimetallic catalysts on different supports were further evaluated in a flow reactor equipped with a gas chromatograph (GC).

2. Experimental

2.1. Preparation of supported catalysts

The Pd–Ni bimetallic catalysts were synthesized by incipient wetness impregnation on five oxide supports: γ-Al_2O_3 (Alfa Aesar, 255 m^2/g), SiO_2 (Alfa Aesar, 120 m^2/g), ZrO_2 (Alfa Aesar, 90 m^2/g), CeO_2 (Sigma Aldrich, nanopowder, particle size < 25 nm), and TiO_2 (Alfa Aesar, Anatase, 15 nm APS Powder, 240 m^2/g). The precursor solutions were prepared by dissolving $Pd(NO_3)_2{\cdot}2H_2O$ (Alfa Aesar) and/or $Ni(NO_3)_2{\cdot}6H_2O$ (Alfa Aesar) in an amount of water just sufficient to fill the pores of 3 g of the support. The precursor solution was then added to the support by dropwise addition and was mixed thoroughly between droplets. The catalysts were dried at 100 °C for 10 h and calcined at 290 °C for 2 h. The sample was heated to 100 °C at 0.4 °C/min and then to 290 °C at 0.8 °C/min. Co-impregnation was used for the bimetallic catalysts to produce greater extent of bimetallic bond formation, as verified previously for supported Pt–Ni catalysts [7]. The composition of the synthesized catalysts was 1.51 wt% Ni–0.91 wt% Pd/γ-Al_2O_3, corresponding to a Ni:Pd atomic ratio of 3:1. The monometallic Pd catalysts (0.91 wt%) were synthesized on γ-Al_2O_3 and SiO_2 to study the Pd–Ni bimetallic effect.

2.2. Catalyst characterization

2.2.1. Transmission electron microscopy (TEM)

TEM measurements were performed using a JEOL2010F equipped with a Schottky field emission gun at 200 keV. All TEM images were taken in the scanning (STEM) mode with a 12 nm camera length and a 1 nm diameter nanoprobe. The TEM samples were prepared by first reducing the catalysts at 450 °C for 1 h, then grinding them into fine powders and suspending them in acetone. In order to fully reduce the Pd–Ni bimetallic particles and to avoid the formation of larger metal particles at higher temperatures, the reduction temperature was chosen based on the TPR results (provided in Fig. R1 in the Supplementary Information). Droplets of the suspension were placed onto a carbon coated copper grid. The grid was dried overnight before loading the sample into the TEM. More than 100 particles were collected for the analysis of particle size distribution.

2.2.2. Pulse CO chemisorption

The number of active sites on each bimetallic catalyst was measured through CO uptake with a ChemBET (QuantaChrome). A quartz reactor was loaded with ~200 mg of catalyst and reduced in 80 sccm of 10% H_2 in He at 450 °C for 1 h. After reduction, the catalyst was held in He at 450 °C for 30 min to remove the remaining H_2 on the surface of the catalysts. Then the catalyst was cooled to room temperature before pulsing CO. The amount of CO flowing out of the reactor was measured with a thermal conductivity detector. Each adsorbed CO molecule was assumed to correspond to one active site, i.e. each Pd or Ni active site was hypothesized to absorb one CO molecule, which provided a means to compare the number of active sites among the various oxide-supported catalysts.

2.2.3. Extended X-ray absorption fine structure (EXAFS)

EXAFS measurements were used to confirm the presence of Pd–Ni bimetallic bonds. Measurements of the Pd K-edge were performed on the X18B beamline at the National Synchrotron Light Source (NSLS), Brookhaven National Laboratory. The catalyst samples were pressed into a pellet with a thickness twice the absorption length to maximize the signal to noise ratio. The catalysts were reduced in-situ in 40 sccm of 50% H_2 in He at 450 °C for 1.5 h, and the EXAFS spectra were collected at room temperature. The EXAFS spectra were calibrated to the Pd K-edge energy from a Pd reference foil.

The X-ray signal was analyzed using the IFEFFIT 1.2.11 data analysis package (Athena, Aretmis, Atoms, and FEFF6) [8,9]. The structural information was obtained by Fourier-transforming the absorbance signal into *R*-space and then fitting each data set to the theoretical standards generated in FEFF6 [10]. The theoretical monometallic photoelectron amplitude and phase were calculated for the bulk Pd fcc structure. The passive electron reduction factor $S_0{}^2$ was found to be 0.878 from fitting the Pd-foil data. The seven parameters used in the fitting procedure were the correction to the edge energy, the coordination numbers of the Pd—Pd and Pd—Ni bonds, corrections to their model interatomic distances, and the mean square deviations in interatomic distances (EXAFS Debye-Waller factors).

2.3. Catalyst evaluation

Flow reactor experiments were performed to evaluate the hydrogenation activity and selectivity of the supported catalysts for 1,3-butadiene hydrogenation. The catalyst was mixed with quartz particles in a ratio of 1:29 (100 mg catalyst and 2.9 g quartz particles) in a fixed-bed reactor. Prior to the reaction, the catalysts were reduced in pure hydrogen at 450 °C for 3 h and then cooled to reaction temperature. The total flow rate of 1,3-butadiene and hydrogen was 9.6 mL/min, and the 1,3-butadiene to hydrogen ratio was 1:4. The reaction temperature range was 30–110 °C. The catalyst was left on stream for 2 h at each temperature to achieve steady state. The outlet stream was analyzed online by a gas chromatograph equipped with a FID detector (GC 7900, Techcomp Ltd.) and an HP-Al/S PLOT column (Agilent, 30 m × 0.53 μm). Only the C_4 species (1,3-butadiene, 1-butene, *trans*-2-butene, *cis*-2-butene and butane) were observed in the outlet, with the gas phase carbon balance above 95%. The selectivity of each product was calculated by dividing its concentration by that of the total products. The butenes selectivity was obtained by summing the selectivities of all butene species.

3. Results

3.1. Catalyst characterization

High angle annular dark field (HAADF) TEM images are presented in Fig. 1 for the Pd–Ni catalysts. The average particle sizes and the CO uptake values are summarized in Table 1. Except Pd–Ni/CeO_2, all catalysts show similar average particle sizes and broad particle size distributions, ranging from ~1 nm up to at least 15 nm; while PdNi/CeO_2 has a much narrower particle size distribution and smaller average particle size of ~3 nm, likely due to the partial alloying of Pd with Ce which has been reported by Bernal et al. [11]. The CO uptake values are consistent with the TEM results. The Pd–Ni catalysts supported on the investigated supports exhibit similar CO uptake values, except that PdNi/CeO_2 has a much higher CO uptake. Combining the TEM and CO uptake results, the values

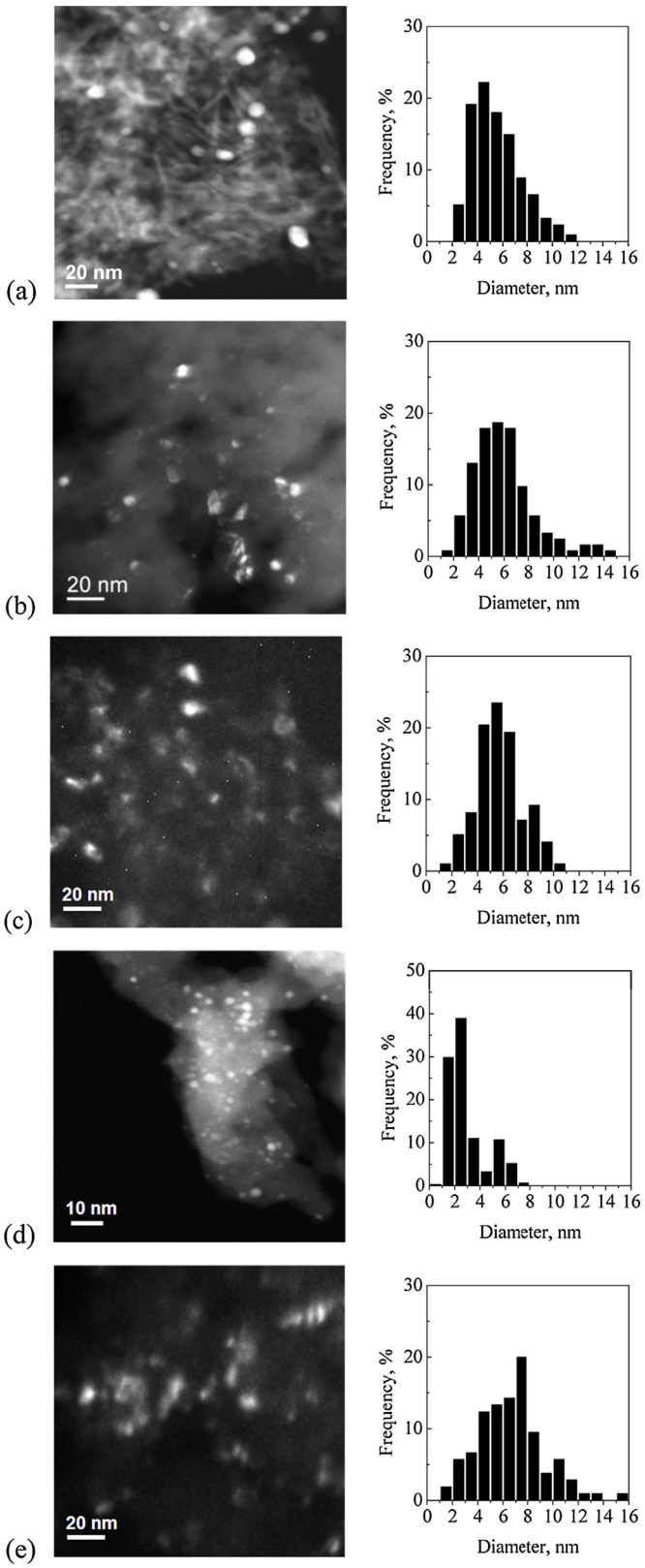

Fig. 1. HAADF TEM images and particle size distributions of (a) γ-Al_2O_3, (b) SiO_2, (c) ZrO_2, (d) CeO_2, and (e) TiO_2.

of CO uptake/$\bar{D}_p$, where $\bar{D}_p$ is the average particle size, are summarized in Table R1 in the Supplementary Information. As shown in the table, the CO uptake/$\bar{D}_p$ values are similar on Al_2O_3, SiO_2, TiO_2 and ZrO_2, (1.4–2.7), while that on CeO_2 is much higher (11.9).

Table 1
Summary of average particle sizes and CO uptake values for supported Pd–Ni catalysts.

Catalyst	Average particle size (nm)	CO-uptake (μmol/g)
Al_2O_3	5.9	15.7
SiO_2	6.3	10.1
CeO_2	3.1	36.8
TiO_2	6.7	9.3
ZrO_2	5.9	16.1

Fig. 2(a) shows the Pd K-edge X-ray absorption near-edge structure (XANES) spectra of the PdNi catalysts supported on γ-Al_2O_3, SiO_2, TiO_2 and CeO_2 [12] before and after reduction, along with the spectra of the Pd foil for reference. The background-subtracted, edge-step normalized and k^2-weighted Pd K-edge EXAFS data ($\chi(k)$) are shown in *R*-space in Fig. 2(b), along with the fits obtained using FEFF6 theory shown in Fig. 2(c). The ZrO_2 supported catalyst is not included because of the poor quality of EXAFS data, likely due to the high background absorbance of Zr (17,998 eV) in the range of Pd (24,350 eV).

Examination of the Pd K-edge XANES and EXAFS reveals information regarding the extent of oxidation of the samples. Relatively intense peaks are present in Fig. 2(a) at 24,350 eV prior to reduction and are attributed to the Pd—O bond, which is confirmed by the peaks at low radial distribution in Fig. 2(b). After reduction in H_2, the spectra are similar to that of the Pd foil in Fig. 2(a), and the Pd–O peaks are no longer present in Fig. 2(b). The Pd–O peaks are replaced by Pd–Ni peaks at slightly larger values of *R*. These changes in the spectra indicate that Pd is in a metallic state after reduction in H_2.

Fig. 2(c) presents the Fourier transformed (*R*-space) data of the reduced catalysts and the associated fits from FEFF6 by including only Pd–Pd and Pd–Ni contributions. The results from the fitting are shown in Table 2. The coordination numbers reveal that bimetallic Pd—Ni bonds are formed in all four catalysts. Table 2 also compares the value of N(Pd–Ni)/[(N(Pd–Ni) + N(Pd–Pd)], which can be used to compare the general trend in the extent of Pd–Ni bimetallic formation. The values are similar on PdNi/CeO_2, PdNi/TiO_2 and PdNi/SiO_2, with PdNi/γ-Al_2O_3 showing a significantly lower value. Such comparison indicates that the extent of Pd–Ni bimetallic formation is much lower on γ-Al_2O_3 than on the other three supports. The relatively small amount of bimetallic bond formation on γ-Al_2O_3 is because a large fraction of Ni atoms form $NiAl_2O_4$ with the supports. For all Pd–Ni catalysts, the EXAFS results show that the Pd–Pd distances are smaller than the Pd–Pd distance on the monometallic catalyst (2.83 Å), while the Pd–Ni distances are larger than the metallic Ni–Ni distance (2.49 Å). These results suggest that Pd–Ni bimetallic bonds are formed on the catalysts because the bimetallic bond lengths are between that of either parent metal. In addition, good fits to the Pd K-edge experimental data could only be obtained by including both Pd–Pd and Pd–Ni contributions in the model, strongly suggesting that bimetallic bonds are present.

In principle, the total coordination numbers from the EXAFS measurements, such as the sum of N(Pd–Pd) and N(Pd–Ni), should correlate with the TEM analysis of particle size. However, quantitatively such correlation is valid only when the particles are uniform, both in physical size and chemical composition. The TEM images reveal that the metals particles have a relatively wide range of size distribution. Therefore TEM results are more reliable and more direct than EXAFS for particle size estimation. The TEM results are also consistent with the trend in the metal dispersion from the CO chemisorption measurements. For example, among the bimetallic catalysts on the four oxide supports, PdNi/CeO_2, is characterized by the smallest particle size in TEM images and the highest metal dispersion in CO chemisorption measurements.

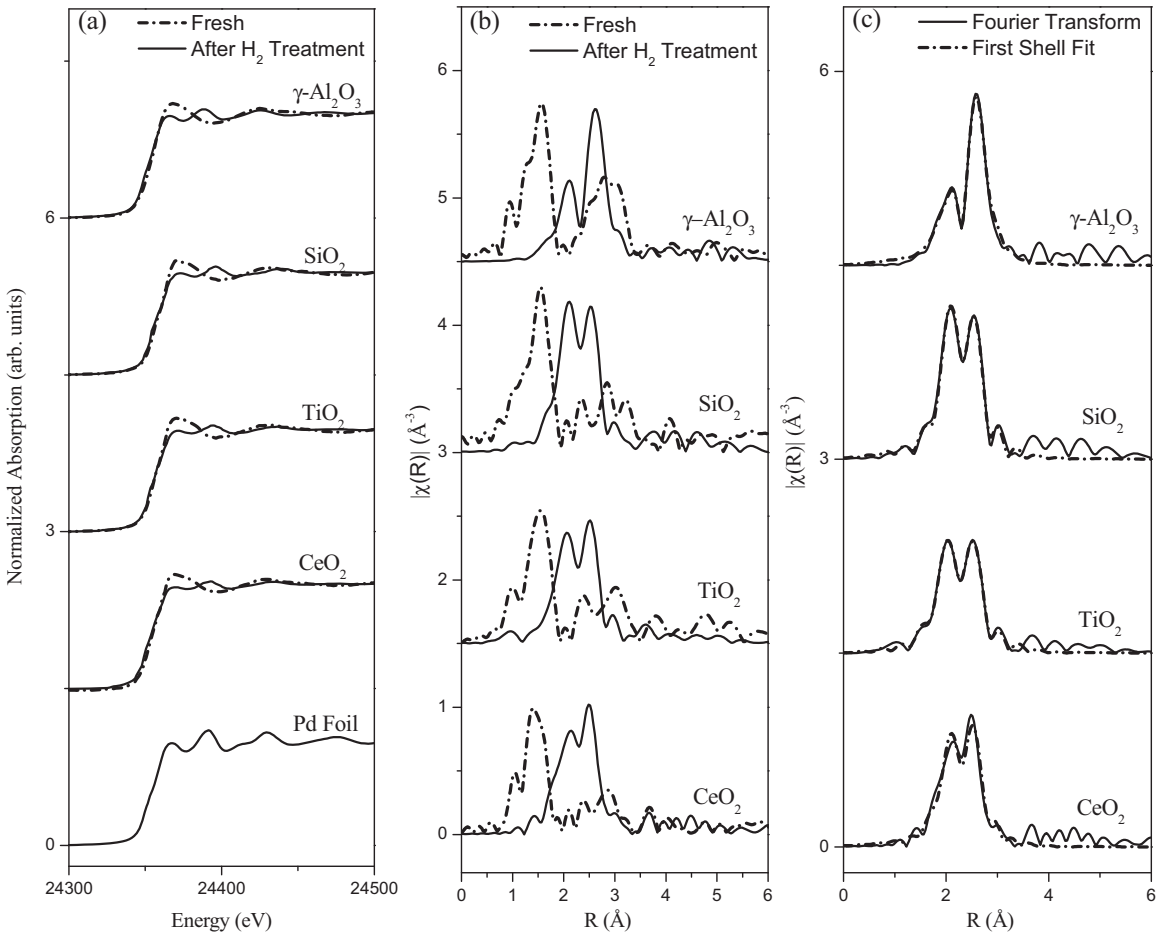

Fig. 2. (a) Pd K-edge XANES spectra before and after reduction; (b) Fourier transformed (magnitude) k^2 weighted EXAFS function ($\chi(k)$) before and after reduction; (c) Pd K-edge Fourier transformed (magnitude) k^2 weighted EXAFS function ($\chi(k)$) after reduction with first shell fit.

3.2. Pd–Ni bimetallic effect

The Pd–Ni bimetallic effect was investigated on γ-Al_2O_3- and SiO_2-supported monometallic and bimetallic catalysts. The Pd catalysts and Pd–Ni bimetallic catalysts were evaluated for the selective hydrogenation of 1,3-butadiene at different temperatures and the results are shown in Fig. 3. The conversions of 1,3-butadiene are plotted as a function of temperature in Fig. 3(a) and (b), and the selectivities to butenes and 1-butene are plotted as a function of conversion in Fig. 3(c) and (d), respectively. The Pd–Ni bimetallic catalysts on both supports show higher conversions and higher 1-butene selectivity than the Pd monometallic catalysts. The selectivity to 1-butene is generally higher on the Pd–Ni bimetallic catalysts than on the Pd catalysts, indicating that the formation of the Pd–Ni bimetallic bond plays a major role in the enhancement of 1-butene selectivity. At conversions below 50%, the selectivity to 1-butene is ~20% higher on PdNi/γ-Al_2O_3 than on Pd/γ-Al_2O_3. Note that on PdNi/γ-Al_2O_3 the 1-butene selectivity decreases rapidly with increasing 1,3-butadiene conversion above 50%, while on Pd/γ-Al_2O_3 it decreases more slowly. Nevertheless the 1-butene selectivity on PdNi/γ-Al_2O_3 remains higher than that on Pd/γ-Al_2O_3 at conversions below 90% and is similar to that on Pd/γ-Al_2O_3 at conversion above 90%. The possible explanation could attribute to the local concentration of the C4 species. At conversions above 90%, the concentration of 1-butene on PdNi/γ-Al_2O_3 becomes very high and the 1,3-butadiene concentration becomes very low. The high concentration ratio of 1-butene and 1,3-butadiene likely enhances the coverage of 1-butene on the surface of Pd–Ni, leading to further hydrogenation and isomerization reactions. As a result, the 1-butene selectivity decreases to the same value with Pd/γ-Al_2O_3 at high 1,3-butadiene conversions. Moreover, the difference between the Pd–Ni and Pd catalysts is larger on SiO_2 than on γ-Al_2O_3. The greater enhancement is most likely from the different extent of Pd–Ni bimetallic bonding. As

Table 2
Summary of EXAFS analysis of Pd K-edge for supported Pd–Ni catalysts.

Catalysts	CeO_2	TiO_2	SiO_2	γ-Al_2O_3
N(Pd–Pd)	4.6 ± 0.4	5.1 ± 0.4	5.8 ± 0.5	8.3 ± 0.7
N(Pd–Ni)	2.3 ± 0.3	2.6 ± 0.7	3.5 ± 0.6	1.4 ± 0.5
R(Pd–Pd) (Å)	2.71 ± 0.01	2.71 ± 0.01	2.70 ± 0.01	2.79 ± 0.01
R(Pd–Ni) (Å)	2.59 ± 0.01	2.58 ± 0.01	2.59 ± 0.01	2.64 ± 0.01
σ^2 (Pd–Pd) (Å^2)	0.008 ± 0.001	0.008 ± 0.003	0.007 ± 0.001	0.010 ± 0.001
σ^2 (Pd–Ni) (Å^2)	0.007 ± 0.001	0.009 ± 0.001	0.008 ± 0.002	0.016 ± 0.004
N(Pd–Ni) + N(Pd–Pd)	6.9	7.7	9.3	9.7
N(Pd–Ni)/[N(Pd–Ni) + N(Pd–Pd)]	0.33	0.34	0.38	0.14

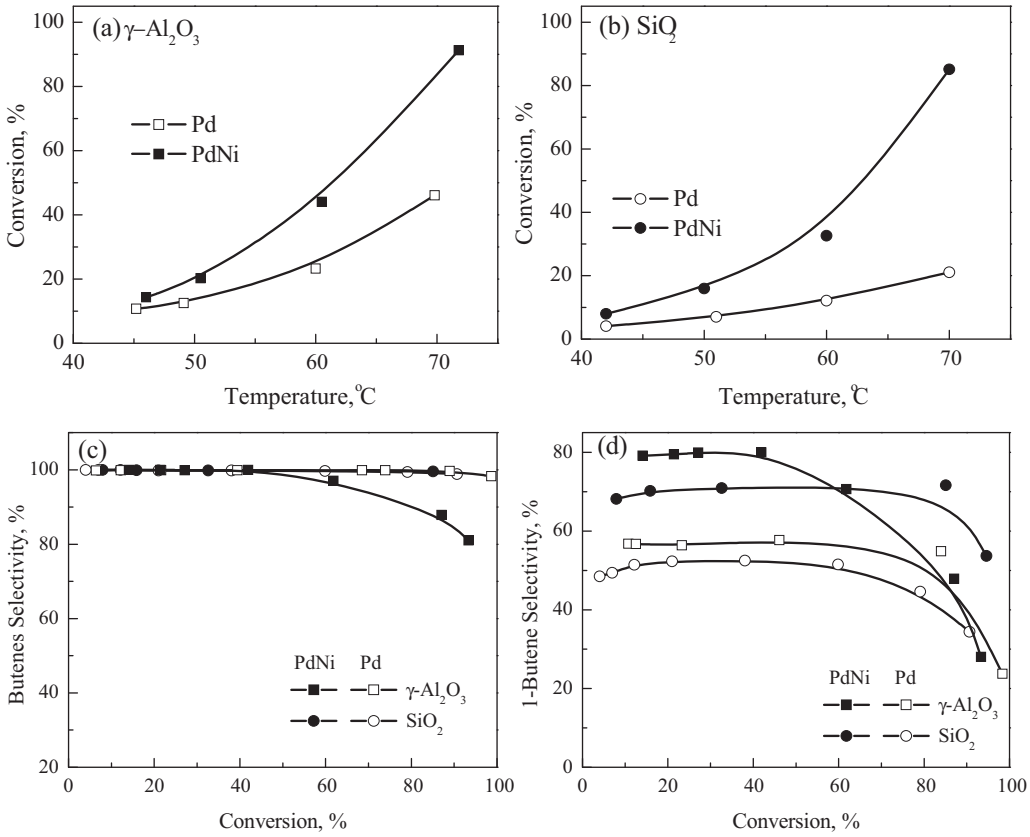

Fig. 3. Conversions of 1,3-butadiene in flow reactor as a function of temperatures for the comparison of Pd and Pd–Ni catalysts on (a) γ-Al_2O_3 and (b) SiO_2; Selectivities to (c) butenes and (d) 1-butene as a function of conversion of Pd–Ni (solid) and Pd (hollow).

summarized in Table 2, the coordination number of Pd–Ni on SiO_2 is 3.5, which is about 2.5 times larger than that on γ-Al_2O_3.

3.3. Support effect

3.3.1. Hydrogenation activity

The Pd–Ni bimetallic catalysts on different supports were evaluated and the activity results are summarized in Fig. 4. Fig. 4(a) shows the 1,3-butadiene conversion on different catalysts as a function of reaction temperature. Based on catalyst weight, the activity of the Pd–Ni bimetallic catalysts follows the trend of CeO_2 > γ-Al_2O_3 ~ SiO_2 > ZrO_2 > TiO_2. However, after normalizing by CO uptake, the turnover frequencies (TOFs, calculated using the data with conversions below 20%) are similar among the five catalysts and the logarithm of TOFs show a linear relationship with the offset reciprocal of the reaction temperatures, except that the TOF value of PdNi/CeO_2 is lower than the average value. The results demonstrate that the bimetallic catalysts on different supports display similar apparent hydrogenation activity regardless of the support nature, suggesting the presence of similar bimetallic active sites on the different oxide supports.

3.3.2. Selectivity

The selectivities to different butene products on the Pd–Ni bimetallic catalysts are shown in Fig. 5. Fig. 5(a) compares the selectivities to butenes on different supports. The butenes selectivities are all close to 100% at conversions lower than 80%; when the conversion approaches 100%, the selectivity decreases slightly over SiO_2, CeO_2, ZrO_2 and TiO_2, but to a greater extent over PdNi/γ-Al_2O_3.

The selectivities to 1-butene, *trans*-2-butene and *cis*-2-butene are plotted as a function of conversion in Fig. 5(b), (c) and (d), respectively. No isobutene was detected during the reaction. Among all the catalysts, the γ-Al_2O_3 supported catalyst gives the highest 1-butene selectivity. At conversions lower than 25%, the selectivity to 1-butene over the Pd–Ni bimetallic catalysts on different supports follows the trend of γ-Al_2O_3 > SiO_2 > CeO_2 ~ ZrO_2 > TiO_2. With increasing conversion, the general trend changes. The 1-butene selectivity on PdNi/ZrO_2 decreases slightly when the conversion increases to above 25% and it falls between that on PdNi/CeO_2 and PdNi/TiO_2. When the 1,3-butadiene conversion further increases to 100%, the selectivity to 1-butene on γ-Al_2O_3 supported catalysts decreases rapidly, while that on SiO_2 supported catalyst decreases only slightly.

The selectivity to *trans*-2-butene shown in Fig. 5(c) follows the trend of TiO_2 > CeO_2 ~ ZrO_2 > SiO_2 > γ-Al_2O_3, which is opposite to that of the selectivity to 1-butene. The selectivity to *cis*-2-butene is similar on different supports, as shown in Fig. 5(d). Because the hydrogenation of 1,3-butadiene only produces 1-butene in a batch reactor as reported before [3], it is very likely that 1,3-butadiene is firstly hydrogenated to 1-butene, and then 1-butene isomerizes to *trans*- and *cis*-2-butenes in the flow reactor. The opposite trend in the selectivities to 1-butene and *trans*-2-butene suggests that most 1-butene isomerizes into *trans*-2-butene. Based on the conclusion above, the oxide support appears to play an important role in the isomerization of 1-butene to *trans*-2-butene.

4. Discussion

4.1. Bimetallic effect

The better performance of the Pd–Ni bimetallic catalysts has been previously demonstrated on single crystal surfaces by both

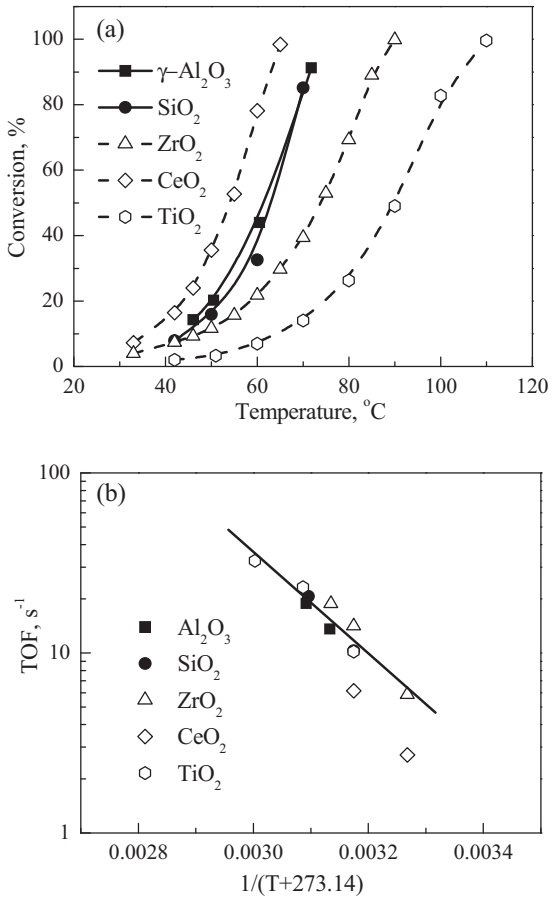

Fig. 4. (a) Conversions and (b) TOFs of 1,3-butadiene in flow reactor at different temperatures for the comparison of Pd–Ni bimetallic catalysts on different supports.

density functional theory (DFT) calculations and surface science experiments, and further verified on the γ-Al_2O_3 supported catalysts using both batch and flow reactors [3]. The present study further confirms the trend by supporting Pd–Ni and Pd onto γ-Al_2O_3 and SiO_2. The bimetallic catalysts show enhancement in both hydrogenation activity and 1-butene selectivity. Moreover, the larger coordination number of Pd–Ni on SiO_2 indicates a greater extent of Pd—Ni bond formation, which is consistent with the greater activity enhancement of PdNi/SiO_2 than PdNi/γ-Al_2O_3 compared with their Pd monometallic counterparts.

4.2. Support effect

4.2.1. Activity

The characterization results from CO chemisorption and TEM are consistent in that PdNi/CeO_2 has higher CO uptake and more uniform small metal particles. The other Pd–Ni supported catalysts show similar particle size distributions and similar CO uptake values. Normalized by CO uptake, the Pd–Ni bimetallic catalysts show similar activity regardless of the support types except that PdNi/CeO_2 shows a slightly lower activity.

Boitiaux et al. [13] reported that the 1,3-butadiene hydrogenation activity strongly depends on the metal dispersion on the Pd monometallic catalysts. The hydrogenation activity is similar when the Pd metal dispersion is lower than 20% and decreases with increasing metal dispersion at above 20%, regardless of the support types (γ-Al_2O_3, α-Al_2O_3 and SiO_2). Goetz et al. [14] also reported that large Pd particles (~6–7 nm) exhibits higher TOF than small Pd particles (~3 nm). These conclusions are consistent with the results in the current study for the Pd–Ni bimetallic catalysts. The investigated Pd–Ni bimetallic catalysts exhibit metal dispersions lower than 20% except PdNi/CeO_2, and they display similar TOFs regardless of the support types. The higher metal dispersion on PdNi/CeO_2 results in slightly lower TOF, which is likely due to the exposure of less active sites on small bimetallic nanoparticles [13]. The electronic effect of the small metal particles makes 1,3-butadiene bind more strongly on the catalyst and accordingly decreases the hydrogenation activity [15].

However, the observation of similar TOF values on different oxide supports is different from the previous study on Pt–Ni bimetallic catalysts [5,6]. It has been reported that the activity of Pt–Ni bimetallic catalysts normalized by CO uptake is higher on γ-Al_2O_3 than on ZrO_2 [5] and TiO_2 [6] for the hydrogenation of 1,3-butadiene in a batch reactor. Moreover, Boitiaux et al. [16] and Primet et al. [17] have demonstrated that the hydrogenation activity of 1,3-butadiene is insensitive to the metal dispersions for Pt catalysts. Because the different activities among the Pt–Ni bimetallic catalysts [5,6] are not from the metal dispersion [16,17], they are possibly from the strong metal-support interaction (SMSI) between the small Pt–Ni nanoparticles and the oxide supports. Even though Pd–Ni might also have SMSI with the corresponding oxide supports, the interaction of Pd with ZrO_2 and TiO_2 might be different from that of Pt with ZrO_2 and TiO_2.

4.2.2. Selectivity

The selectivity to 1-butene over the Pd–Ni bimetallic catalysts on different supports follows the trend of γ-Al_2O_3 > SiO_2 > CeO_2 ~ ZrO_2 > TiO_2 at low conversion of 1,3-butadiene. The different performance reflects the different support modification on Pd–Ni bimetallic catalysts. However, the selectivity performance varies from low to high 1,3-butadiene conversions.

It has been reported that the selectivities to butene species are independent of the metal dispersion [13], therefore the nature of supports, as well as the interaction between metal and support, should be responsible for the different performance in 1-butene selectivity among Pd–Ni catalysts on different supports. Several support effects could affect the selectivity of 1,3-butadiene hydrogenation, i.e., metal-support interaction, oxide defect, and geometric/electronic effect.

SMSI has been reported to exist on the TiO_2, CeO_2 and ZrO_2 supported catalysts if reduced at temperatures higher than 500 °C [11,18,19], and that the SiO_2 and Al_2O_3 supported catalysts exhibit weaker metal-support interactions [19–21]. By forming bimetallic metal bond, the required reduction temperature for SMSI could be reduced (see Fig. 3 in Ref. [22]). As a result, the Pd–Ni bimetallic catalysts on TiO_2, CeO_2 and ZrO_2 probably present SMSI. The results show that the catalysts on the oxide supports with possible SMSI or possible oxide defects generally give lower 1-buene selectivity. The trend of 1-butene selectivity indicates that the possible SMSI effect decreases the 1-butene selectivity for the Pd–Ni bimetallic catalysts. The difference in 1-butene selectivity might also come from the oxide defects. TiO_2 and CeO_2 are reducible supports and high-surface area ZrO_2 may have oxygen defects during reaction. The apparent correlation between the oxygen defects and the lower 1-butene selectivity suggests that the oxygen defects are also a possible reason for the lower 1-butene selectivity.

Different support might also affect the geometric and electronic properties on the Pd–Ni bimetallic catalysts [23]. According to the EXAFS results, the coordination numbers of Pd–Ni on different supports are different, leading to different particle composition on Pd–Ni bimetallic particles. On the other hand, TEM results revealed that the particle sizes were similar on all supports except on CeO_2. The EXAFS and TEM results suggest that the bimetallic composition,

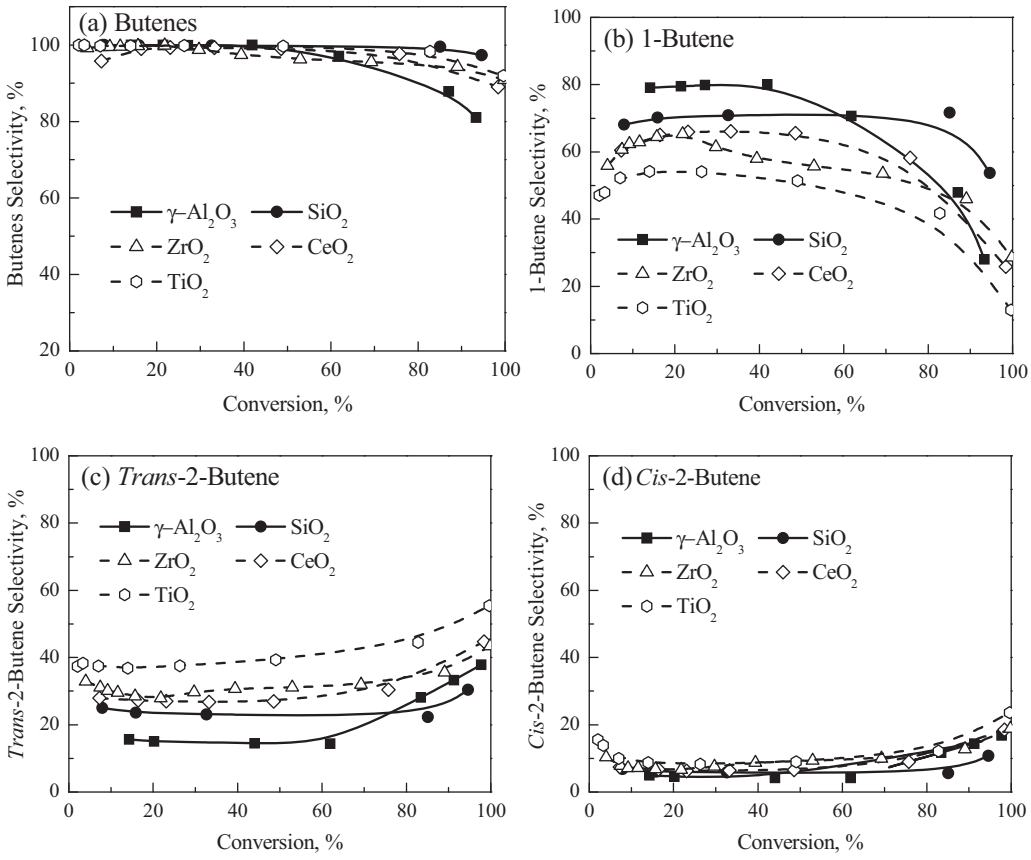

Fig. 5. Selectivities to (a) butenes, (b) 1-butene, (c) *trans*-2-butene and (d) *cis*-2-butene over Pd–Ni bimetallic catalysts on different supports.

not the physical size of the particles, plays a significant role for the selectivity in 1,3-butadiene hydrogenation.

5. Conclusions

Hydrogenation of 1,3-butadiene has been studied on the Pd–Ni bimetallic catalysts supported on γ-Al_2O_3, SiO_2, CeO_2, ZrO_2 and TiO_2 using a flow reactor. The Pt–Ni bimetallic catalysts on γ-Al_2O_3 and SiO_2 are compared with the Pd catalysts to study the bimetallic synergy effect. The results show that the Pd–Ni bimetallic catalysts have both higher hydrogenation activity and higher 1-butene selectivity than the Pd catalysts. The bimetallic synergy effect is more significant on SiO_2 than on γ-Al_2O_3, i.e. the enhancement by Ni addition is greater on SiO_2 than on γ-Al_2O_3, which is consistent with the greater extent of Pd–Ni bimetallic bond formation on SiO_2.

The chemical nature of the supports influences the bimetallic metal particle structures, but does not affect the hydrogenation activity. Only the metal particle size affects the turnover frequency. On the other hand, the 1-butene selectivity depends on the nature of supports. The possible SMSI effect and oxygen defects are possible reasons for the lower 1-butene selectivity on PdNi/CeO_2, PdNi/ZrO_2 and PdNi/TiO_2.

Acknowledgements

The work at Columbia University and Brookhaven National Laboratory was carried out under Contract No. DE-AC02-98CH10886 with the U.S. Department of Energy, Office of Basic Energy Sciences. R. Hou was sponsored by the China Scholarship Council. T.F. Wang was supported by Program for New Century Excellent Talents in University of China (NCET-12-0297).

Appendix A. Supplementary data

Supplementary data associated with this article can be found, in the online version, at http://dx.doi.org/10.1016/j.apcata.2014.11.001.

References

[1] A. Hugon, L. Delannoy, J.M. Krafft, C. Louis, J. Phys. Chem. C 114 (2010) 10823–10835.
[2] J.A. Alves, S.P. Bressa, O.M. Martinez, G.F. Barreto, Chem. Eng. J. 99 (2004) 45–51.
[3] R. Hou, W. Yu, M.D. Porosoff, J.G. Chen, T. Wang, J. Catal. 316 (2014) 1–10.
[4] S. Qi, B.A. Cheney, R. Zheng, W.W. Lonergan, W. Yu, J.G. Chen, Appl. Catal. A 393 (2011) 44–49.
[5] W.W. Lonergan, T. Wang, D.G. Vlachos, J.G. Chen, Appl. Catal. A 408 (2011) 87–95.
[6] T. Wang, G. Mpourmpakis, W.W. Lonergan, D.G. Vlachos, J.G. Chen, Phys. Chem. Chem. Phys. 15 (2013) 12156–12164.
[7] W.W. Lonergan, D.G. Vlachos, J.G. Chen, J. Catal. 271 (2010) 239–250.
[8] M. Newville, J. Synchrot. Radiat. 8 (2001) 322–324.
[9] B. Ravel, M. Newville, J. Synchrot. Radiat. 12 (2005) 537–541.
[10] J.J. Rehr, R.C. Albers, Rev. Mod. Phys. 72 (2000) 621–654.
[11] S. Bernal, J. Calvino, M. Cauqui, J. Gatica, C. Larese, J. Pérez Omil, J. Pintado, Catal. Today 50 (1999) 175–206.
[12] M.D. Porosoff, J.G. Chen, J. Catal. 301 (2013) 30–37.
[13] J.P. Boitiaux, J. Cosyns, S. Vasudevan, Appl. Catal. 6 (1983) 41–51.
[14] J. Goetz, M.A. Volpe, R. Touroude, J. Catal. 164 (1996) 369–377.
[15] W.W. Lonergan, X. Xing, R. Zheng, S. Qi, B. Huang, J.G. Chen, Catal. Today 160 (2011) 61–69.
[16] J.P. Boitiaux, J. Cosyns, E. Robert, Appl. Catal. 32 (1987) 145–168.
[17] M. Primet, M. Elazhar, M. Guenin, Appl. Catal. 58 (1990) 241–253.
[18] S. Tauster, S. Fung, R. Garten, J. Am. Chem. Soc. 100 (1978) 170–175.
[19] E.V. Benvenutti, L. Franken, C.C. Moro, C.U. Davanzo, Langmuir 15 (1999) 8140–8146.
[20] J.H. Kang, E.W. Shin, W.J. Kim, J.D. Park, S.H. Moon, J. Catal. 208 (2002) 310–320.
[21] S.J. Tauster, S.C. Fung, J. Catal. 55 (1978) 29–35.
[22] M. Kang, M.W. Song, K.L. Kim, React. Kinet. Catal. Lett. 75 (2002) 177–183.
[23] G.L. Haller, D.E. Resasco, Adv. Catal. 36 (1989) 173–235.